Published in final edited form as:
Neuroimage. 2009 April 1; 45(2): 360–369. doi:10.1016/j.neuroimage.2008.12.022.

Combined magnetic resonance and fluorescence imaging of the living mouse brain reveals glioma response to chemotherapy

Corey M. McCann[1], **Peter Waterman**[1,2], **Jose-Luiz Figueiredo**[1,2], **Elena Aikawa**[1], **Ralph Weissleder**[1,2], and **John W. Chen**[1,2]

[1]Center for Molecular Imaging Research, Massachusetts General Hospital, 185 Cambridge Street, Boston, Massachusetts 02114, USA.

[2]Center for Systems Biology, Massachusetts General Hospital, 185 Cambridge Street, Boston, Massachusetts 02114, USA.

Abstract

Fluorescent molecular tomographic (FMT) imaging can noninvasively monitor molecular function in living animals using specific fluorescent probes. However, macroscopic imaging methods such as FMT generally exhibit low anatomical details. To overcome this, we report a quantitative technique to image both structure and function by combining FMT and magnetic resonance (MR) imaging. We show that FMT-MR imaging can produce three-dimensional, multimodal images of living mouse brains allowing for serial monitoring of tumor morphology and protease activity. Combined FMT-MR tumor imaging provides a unique *in vivo* diagnostic parameter, protease activity concentration (PAC), which reflects histological changes in tumors and is significantly altered by systemic chemotherapy. Alterations in this diagnostic parameter are detectable early after chemotherapy and correlate with subsequent tumor growth, predicting tumor response to chemotherapy. Our results reveal that combined FMT-MR imaging of fluorescent molecular probes could be valuable for brain tumor drug development and other neurological and somatic imaging applications.

INTRODUCTION

Combined functional and anatomical imaging (for example, positron emission tomography-computed tomography, PET-CT) has significantly improved clinical diagnosis, staging, and patient prognosis for many oncological diseases (Lardinois et al., 2003; Otsuka et al., 2007; Veit-Haibach et al., 2006; Weber et al., 2008). Another functional modality, near-infrared fluorescence (NIRF) imaging is well suited for visualizing molecular activity since background fluorescence is typically low (Weissleder and Ntziachristos, 2003), simultaneous visualization of multiple targets is possible (Nahrendorf et al., 2007) and specific probes are easily conjugated to fluorescent molecules (Bremer et al., 2003). To that end, there currently exists a multitude of specific and activatable fluorescent probes for imaging tumors (Kelloff et al., 2005), cardiovascular diseases (Jaffer et al., 2006), arthritis (Izmailova et al., 2007) and neurological diseases (Hintersteiner et al., 2005; Nesterov et al., 2005), among other biological phenomena.

Fluorescent molecular tomographic (FMT) imaging is an imaging technique that utilizes mathematical models describing photon propagation in tissues to allow for 3D reconstruction of fluorescence in living animals at centimeter depth (Ntziachristos et al., 2002a; Ntziachristos

Correspondence to: John W. Chen, Center for Molecular Imaging Research, Center for Systems Biology, Massachusetts General Hospital, Harvard Medical School, Room 5406 CNY-149, 13th Street, Charlestown, MA 02129, phone: 617-643-3778; fax: 617-726-5708, email: E-mail: chenjo@helix.mgh.harvard.edu.

et al., 2005; Ntziachristos et al., 2004; Ntziachristos et al., 2002c). For tomography, multiple points (sources) are illuminated on the mouse tissue surface and diffuse light patterns are collected in transillumination mode using a CCD camera. Each source-detector pair represents a different projection through the tissue and these measurements are then combined in a tomographic scheme utilizing a normalized Born approach (Graves et al., 2005). Fluorescence measurements are obtained using appropriate filters allowing for multispectral reconstructions. This technique has been validated for a wealth of imaging agents including magnetofluorescent nanoparticles (Montet et al., 2005), fluorescently conjugated peptides (von Wallbrunn et al., 2007), fluorescent proteins (Zacharakis et al., 2005) and activatable imaging probes (Ntziachristos et al., 2002c). Unlike traditional planar fluorescence imaging techniques that suffer from nonlinear depth-dependent photon absorption within the subject (Ntziachristos et al., 2003), FMT is quantitative and allows for measurements of fluorophore concentration throughout living animals (Graves et al., 2005).

However, as NIRF and FMT imaging are macroscopic imaging methods, precise anatomical context for the molecular activity information and details of the surrounding non-near infrared fluorescent tissue are often not easy to obtain or visualize. In contrast, magnetic resonance (MR) imaging, while more difficult to harness for molecular applications because of lower probe detection sensitivity and difficulties associated with creating specific and activatable MR agents, is able to provide high resolution three dimensional (3D) structural images. Therefore, the ability to combine these two imaging modalities to achieve detailed structural and functional data sets would be of high value to many biological, preclinical, and in the future, clinical applications such as detailed assessment of tumor physiology and identification of vulnerable foci in neurodegenerative diseases.

In this study, we describe, validate, and apply image processing and registration methods to combine 3D, quantitative, tomographic fluorescence and magnetic resonance (FMT-MR) imaging in longitudinal studies of the mouse brain. Similar to PET-CT imaging, FMT-MR imaging can utilize highly specific molecular probes to study molecular and cellular phenomenon with detailed anatomical correlation. An additional advantage of FMT-MR is that there is no radiation exposure to the subject or the user. We show that this technique can be applied to the imaging of brain tumors, tracking functional and volumetric data over time to monitor tumor growth and response to chemotherapy. Moreover, by obtaining accurate tumor volume with MR and measuring tumor function and response with a fluorescent probe for protease activity, we are able to quantify and track changes over time in living mice, noninvasively detecting histological changes in tumors. We found that the protease activity concentration (PAC) derived from the combined imaging method significantly and rapidly increases following the administration of a clinical chemotherapeutic agent, temozolomide (TMZ). Early changes in PAC correlate well with subsequent tumor growth and thus allowed for predictions of tumor response to chemotherapy. These results provide new methods for detailed structural and functional imaging of living animals. While this method is currently limited to small animal imaging, this study highlights the utility of combined imaging for drug development and preclinical trials.

METHODS

Mouse models

The protocol for animal experiments was approved by the institutional animal care committee. A total of 65 male mice age 8–12 weeks were used for this study.

A. Phantom study (n=20)—Fluorescent phantoms were created by filling small plastic tubes (|1mm in diameter) with a NIRF fluorophore. Fluorescent phantoms were filled with VivoTag 680 (VisEn Medical, Bedford, MA) and magnetofluorescent phantoms were filled with cross-linked iron oxide conjugated to VivoTag 680 (synthesized by the CMIR Chemistry Core). Mice were anesthetized with ketamine (90 mg/kg) and xylazine (10 mg/kg) and the surgical site sterilized with betadine/ethanol before surgery. A midline incision was made through the skin overlying the cranium. A small hole was made in the skull using a bone drill and phantoms were inserted stereotactically. Holes in the skull were covered with bone wax and the scalp was sutured (7–0 Ethicon, Sommerville, NJ). Animals were allowed to recover and then returned to their cages.

B. Brain tumor growth study (n=20)—For brain tumor imaging, U87, a human glioma cell line, was obtained from the American Tissue Culture Collection (Manassas, VA, USA). U87 cells were maintained in MEM (Invitrogen, Carlsbad, CA, USA) supplemented with 10% fetal bovine serum. To generate a fluorescent glioma cell line, U87 cells were transfected with a DsRedII plasmid that incorporated a neomycin resistance gene (Clontech, Mountain View, CA, USA). Stably transfected cells were selected with G418, single cells were cloned, and clones expressing the construct in all cells were identified.

For tumor cell implantation, nude mice (Cox-7, Massachusetts General Hospital, Boston, MA, USA), 20–25 g, were anesthetized and prepared as above. Tumor cells were implanted 2 mm posterior and 2 mm lateral to the bregma. 4–6μl of a cell suspension containing 10^6 cells was injected at a depth of 2mm from the skull surface. The injection was done slowly over the course of 10 minutes. The burr hole was filled with bone wax (Ethicon, Sommerville, NJ, USA) and the scalp was closed with sutures.

C. Chemotherapeutic treatment study (n=25)—For chemotherapy treatment, animals were allowed to recover for 1 week after tumor cell injection. TMZ capsules (Temodar; Schering-Plough, Kenilworth, NJ, USA) were opened and the drug contained within was suspended in dimethyl sulfoxide (DMSO) before intraperitoneal injection of a DMSO/temodar solution each day for 5 days. The low dose treatment regimen was 20 mg/kg and the high dose regimen was 100mg/kg.

Imaging

Twenty-four hours before tumor imaging, mice were injected intravenously with 2 nmoles of ProSense680 (VisEn Medical, Bedford, MA, USA). For FMT imaging, animals were anesthetized with ketamine/xylazine and hair covering the area to be imaged was removed. Fluorescence neuroimaging was conducted in a VisEn Medical FMT Fluorescence Molecular Tomography system (Bedford, MA, USA). This system includes two near-infrared laser diodes at 670 nm and 745 nm and matched emission filters at 700 nm and 780 nm respectively. Images were captured using a low-noise TE cooled CCD camera with air assist. This system uses a refractive index matching fluid to surround the animal. We used lanolin to cover the animal's mouth and the nostrils were suspended above the fluid line to allow the animal to breath. To avoid erroneous signals from the air-fluid interface, the area to be imaged was always more than 1cm below the fluid level. We should note that these steps may be skipped with the new generation of FMT scanners that do not need the index matching fluid. Once the mouse was positioned in the imaging chamber, reflectance images were captured in white light and fluorescence. Typical scanning times were 5 minutes per animal. A scan field was selected, encompassing the skull of the mouse, and tomography was carried out. Two sets of scans were acquired for each tomographic imaging session (an excitation scan and a fluorescence scan). Scan field was 15mm × 15mm × 13mm (WxHxD), with a matrix size of 96 × 96 × 26, resulting in voxel dimensions of 0.156mm × 0.156mm × 0.5mm. The data from these scans were analyzed using a normalized Born approach, and 3-dimensional data sets were generated (Graves et al., 2005; Kak and Slaney, 1988). Briefly, emission images, corrected for filter bleed-through of excitation light were divided by the excitation images. Fluorescence measurements less than ten standard deviations above the noise level of the emission acquisitions were ignored. For tomographic data analysis, volumes of interest (VOIs) were selected by drawing a region of interest in each of the 3 imaging planes (X, Y, Z) utilizing the FMT software, with and without referencing the MRI data.

MR imaging was performed immediately (within a few minutes) after the completion of FMT imaging. Animals were imaged with a 7T Bruker Pharmascan MR scanner (rapid acquisition relaxation-enhanced (RARE) T_2-weighted sequence: TR=3500 ms, TE=75 ms, twelve repetitions were acquired and averaged, acquisition time 11 minutes and 12 seconds, matrix size 256 × 256, field of view 2.5 × 2.5 cm, slice thickness 0.5 mm, 16 sections acquired; RARE T_2-weighted 3D sequence: TR=2000 ms, TE=70 ms, one signal acquired, acquisition time 1 hour 8 minutes 16 seconds, matrix size 256 × 128 × 128, field of view 3.0 × 2.5 × 2.0 cm). RARE T_2-weighted 2D and 3D images and RARE T_1-weighted (TR=800, TE=13; four repetitions were acquired and averaged, acquisition time of 6 minutes 57 seconds, matrix size 256 × 192, field of view 2.5 × 2.5 cm, slice thickness 0.8 mm, and 18 sections were acquired) images were acquired before and after the bolus intravenous administration of 0.3 mmol/kg GdDTPA (Magnevist; Berlex, NJ, USA) via the tail vein using a 32 gauge needle. Tumor volume was measured by manually outlining regions of gadolinium enhancement on individual images and calculating an area measurement. This area was then multiplied by the slice thickness to estimate a volume. Volumes calculated for image sections spanning the tumor were added to calculated tumor volume.

Fluorescence tomography/MR image fusion

To fuse the FMT and the MR images, we performed co-registration by transforming the 3D FMT data sets in the XY-, XZ-, and YZ-planes. For each plane, we first created projection data in the appropriate plane. We then identified landmarks in the FMT dataset, and on the corresponding white light reflectance image in the case of the XY-plane. Suitable markers included ears, eyes, snout, fluorescent phantoms, and tumor foci. These same landmarks were then also identified on the corresponding MR images. From these landmark data, an angle of rotation and a translation distance from the center of the FMT image were identified to align the landmarks between the two imaging data sets. These rotation and translation parameters were then applied to each of the FMT images. We also performed correction in the XZ-plane by identifying the top of the skull in both the FMT and MRI data sets. On the FMT images, the top of the skull touches the glass plate in the imaging device, and consequently, the top of the skull begins on image plane #*2*. Therefore, we cropped both datasets so that the top of the skull is the first image in the image stack. After rotation and translation have been performed for these three orthogonal planes, the FMT data were re-projected onto the XY-plane and registration was verified. If necessary, this procedure was repeated until we have achieved coregistration. While we matched the same slice thickness between FMT and MRI images (0.5 mm), the matrix size of FMT is inherently smaller than that of MRI. Therefore, the matrix size of the FMT images was linearly scaled to match the matrix size of MRI images. Pseudocolored single sections and projections were created using the software Metamorph (version 6.3, Downingtown, PA, USA, www.moleculardevices.com/pages/software/metamorph.html). Final image fusion was carried out using the three-point triangulation algorithm in OsiriX (version 2.7.1, Geneva, Switzerland, www.osirix-viewer.com).

Protease activity concentration (PAC) was calculated by dividing the total protease activity by tumor volume (Eq. 1):

$$PAC=\frac{Total\ brain\ protease\ activity\ (FMT)}{Tumor\ volume\ (MRI)}$$

Total protease activity was measured by using FMT to image the total amount of ProSense fluorescence in a volume of interest containing the entire mouse brain by referencing the MRI data. Tumor volume was measured by manually outlining tumor margins in individual MR images from brains of gadolinium treated animals. The area of enhancement was multiplied by the slice thickness to estimate a volume. Total tumor volume was then calculated by adding single section tumor volumes for image sections spanning the tumor.

Tumor Histology

Following *in vivo* imaging, animals were sacrificed for histology. For direct visualization of ProSense 680 and DsRedII expressing tumor cells, animals were intracardially perfused with a solution of 4% paraformaldehyde (PFA) in phosphate buffered saline (PBS), the brains removed and then fixed in 4% PFA for 24hrs. Brains were mounted in agarose and sectioned at 50μm using a vibratome (Leica Microsystems, Bannockburn, IL, USA). Brain sections were mounted in Vectashield (Vector Laboratories, Burlingame, CA) underneath a coverslip and imaged with a CCD camera (Retiga SRV, QImaging, Burnaby, BC, Canada) coupled to an upright microscope (Zeiss Axioplan II, Thornwood, NY, USA). For immunohistochemical analyses of the tumors, fresh-frozen brain specimen were prepared over dry ice in isopentane in the embedding media O.C.T. (Sakura Finetek, Torrance, CA, USA). Five μm cryosections of the frozen tissues were examined for the presence of macrophages/microglia (mac-3, BD Biosciences, CA), neutrophils (NIMP-R14, Abcam, Cambridge, MA), apoptosis (TUNEL kit, Chemicon, Temecula, CA), and proliferation (rabbit polyclonal Ki67, Abcam, Cambridge, MA). The avidin-biotin peroxidase method was employed. The reaction was visualized with 3,3'-diaminobenzidine (DAB) method (Sigma Chemical, St. Louis, MO). All sections were counterstained with hematoxylin. Hematoxylin-eosin staining was also performed to study the overall morphology. Images were captured with a digital camera (Nikon DXM 1200-F, Nikon Inc., Melville, NY).

Statistical analysis

Results are expressed as mean±standard deviation. The data sets were tested for normality using the Kolmogorov-Smirnov test with the Dallal-Wilkinson-Lilliefor correction and for equality of variances using the F test. Data were compared using the unpaired 2-tailed *t*-test. If either the normality or equality of variances was rejected, the nonparametric Mann-Whitney test was used. A p-value <0.05 was considered to indicate a statistically significant difference. Analysis was performed using GraphPad Prism 4.0c (GraphPad Software, Inc., San Diego, CA, USA).

RESULTS

Fluorescence tomography imaging of the murine brain

FMT has been extensively used to image the abdomen, chest and extremities in living mice (Ntziachristos et al., 2005), but has been used to a lesser extent in neuroimaging. Brain imaging has been difficult, in part, because most first generation FMT systems, like ultrasound systems, use a refractive index matching fluid that surrounds the tissues to be imaged. When imaging targets in the head, this fluid can potentially suffocate the animal unless intubated. We therefore first developed methods to submerge living mice in matching fluid while allowing the animal to remain breathing (Figure 1a). To ask whether this submersion technique allowed for fluorescence imaging of the brain, we implanted NIRF phantoms into the brains of living mice and then imaged them with FMT (Figure 1b–d and see Figure 1b for a description of fluorescent phantoms).

Using tomographic fluorescence imaging, fluorescent phantoms were resolvable as unique fluorescent foci (Figure 1d). The location of the fluorescence signal was comparable to the location of fluorescence that we observed from more traditional planar imaging techniques (Figure 1c). Furthermore, the size of the phantom (Figure 1d, dashed black circle), as assessed by post mortem dissection, was reflected by the size of the fluorescent focus on tomographic imaging (Figure 1d). More importantly, FMT was also able to assess fluorophore concentration and phantom depth (Figure 1d and inset).

Combined fluorescence and magnetic resonance imaging *in vivo*

To assess the feasibility of combined fluorescence and MR imaging, we implanted magnetofluorescent phantoms (see Figure 1b) into the brains of living mice and then imaged animals with both FMT and MR. Phantoms were visible as hypointense regions on T2-weighted MR images (Figure 2c, colorized red). When we imaged the same animals with FMT, we detected a single fluorescent focus. Using landmarks visible in both datasets (Figure 2a, b), we were able to map the fluorescence data onto the region in the MR image known to contain the magnetofluorescent phantom to create a fused data set (Figure 2d–h and Figure S1).

We next determined whether combined imaging could be applied to image multiple fluorescent objects in the same brain. When we implanted two magnetofluorescent phantoms, two discrete foci were detected (Figure 2e). Phantom distance as calculated by FMT correlated with MRI measurements as small as 4mm (Figure 2f). By implanting three magnetofluorescent phantoms, we were able to test the three dimensional accuracy of combined imaging. Animals with three implanted phantoms showed three discrete regions of fluorescence intensity corresponding to three hypointense regions on MRI. These three points could be triangulated in 3D space to create fully three dimensional fused data sets (Figure 2g, h).

Combined imaging of brain tumors *in vivo*

Combined imaging could provide an ideal tool for monitoring biological processes and localizing these processes to discrete regions of the brain over time. To that end, we chose to image protease activity in brain tumors since there are currently existing NIRF probes for protease activity (Blum et al., 2005; Jiang et al., 2004; Weissleder et al., 1999) and tumor proteases are thought to play a role in tumor growth, invasiveness and metastasis (Bindal et al., 1994; Koblinski et al., 2000; Sloane, 1996). We stereotactically implanted human glioblastoma cells (U87) into the brains of living mice and imaged over time with FMT-MR. After systemic GdDPTA (gadolinium) injection, tumors appeared hyperintense on T_1-weighted MR images relative to the surrounding brain parenchyma, delineating tumor margins (Trehin et al., 2006). We also injected animals with ProSense, a chemical probe that exhibits specific NIR fluorescence after cleavage by lysosomal cysteine and serine proteases (Weissleder et al., 1999).

By FMT-MR imaging of these imaging agents we were able to map protease activity onto brain anatomy (Figure 3a). Combined imaging revealed that ProSense signal emanated from the region of the brain bearing the tumor (Figure 3a). Furthermore, by serially imaging animals with ProSense, we were able to quantify changes in protease activity over time (Figure 3a, compare day 7 versus day 13). We observed that tumor protease activity increased rapidly in small tumors (defined as days 7–10 post implantation, Figure 3c, d) and more slowly and in some cases decreased over time in larger tumors (defined as days 10–13 and 13–22, Figure 3c, d). By utilizing the ability of FMT to accurately measure the amount of fluorophore and gadolinium-enhanced MR to accurately measure tumor volume, we were able to calculate the ratio of ProSense fluorescence to tumor volume, thus reporting the protease activity concentration (PAC). We found PAC was relatively constant between one and two weeks post tumor implantation but values were significantly decreased by three weeks after implantation, regardless of tumor size (Figure 3e).

It is important to note that the parameter mean fluorochrome concentration (MFC) computed from FMT alone is different from PAC in that MFC is generated by placing a volume-of-interest (VOI) over the fluorescence signal instead of the actual tumor, and minor variability in the size and placement of the VOI could result in substantially different values. On the other hand, PAC is derived from the total fluorescence signal that is found within the brain margins defined by MRI from the image fusion, and computed using the true tumor volume measured on the MR images. As a result, examination of the MFC calculated without referencing MRI data in general underestimated the concentration and was unable to distinguish between the treated and control animals at any time point (Figure S2).

To test the accuracy of FMT-MR tumor imaging we performed histopathological analyses following live animal imaging. Consistent with combined imaging results suggesting ProSense signal originating from the tumor (Figure 3a), at early time points after tumor cell implantation, when tumors were relatively small, we observed ProSense fluorescence within the confines of the tumor but not outside of the tumor (Figure 3b, black and white arrows respectively). At later time points when the tumor was much larger, ProSense signal was still restricted to the tumor. However, in larger tumors, necrotic, pseudopalisade-resembling regions within the tumor (Brat et al., 2004) lacked ProSense signal (Figure S3) and ProSense labeling was less intense (840+/−160 for small tumors vs. 480+/−230 for large tumors, $p=0.0027$). These two changes provide a histological explanation for the decreases in PAC detected by combined imaging. The fact that changes in PAC mirrored observable changes in tumor histology suggests the ability of FMT-MR imaging to detect subtle changes in the cellular milieu of brain tumors *in vivo*.

Combined imaging of chemotherapy *in vivo*

In preclinical trials and clinical medicine it can often be difficult to know whether a chemotherapy treatment is efficacious. Since combined imaging was able to detect variations in tumor structure and function (see above), we next tested whether it could be applied to detect the effects of chemotherapy on solid tumors. Again, we implanted glioma (U87) cells into the brains of nude mice. One week later, we systemically administered the chemotherapeutic TMZ, once per day for 5 days (a course commonly used in clinical therapy) (Schiff, 2007). We then monitored the gliomas using FMT-MRI.

We were able to image tumor size, localization and protease activity *in vivo* throughout the chemotherapeutic course (Figure 4a and b). It was apparent that TMZ treatment was capable of arresting tumor growth for at least 2 weeks following the onset of treatment (Figure 4e, red diamonds). However, MR imaging was inadequate at detecting early changes by tumor volume. During and immediately after chemotherapy, tumor volume, measured from gadolinium enhanced MRI, was not significantly different between the treated and control groups ($p>0.05$ for both days 3 and 6 post treatment onset; Figure 4e, compare red and blue diamonds at days 3 and 6). In contrast, FMT appeared to be able to demonstrate differences between control and treatment groups by the third day of the chemotherapeutic course ($p=0.016$; Figure 4f, compare red and blue diamonds at day 3). However, this difference was lost by the end of the chemotherapeutic course ($p>0.05$), most likely because the treatment causes complex biological interactions between the host and the tumor. In contradistinction to both MRI and fluorescence imaging alone, results from the combined imaging was capable of unequivocally detecting early chemotherapy induced changes: by the end of treatment, PAC was significantly different than control values ($p=0.0068$; Figure 4g, compare red and blue diamonds at day 6), and this difference persisted for the rest of the study.

We performed histopathological analyses on control and chemotherapy treated animals to assess if changes in PAC reflected changes in tumor histology. As shown above, in untreated tumors, ProSense was found within the margins of the tumor but was excluded from brain parenchyma not containing tumor cells (Figure 4c, see blue labeling in red region). In contrast, by 6 days after the initiation of chemotherapy, ProSense labeling was present both within the tumor (Figure 4d, white arrow) as well as outside the tumor (Figure 4d, black arrows). ProSense fluorescence within the confines of the tumor was also more intense after chemotherapy (1420 +/−120 for treated tumors vs. 560+/−230 for untreated tumors, $p<0.0001$; Figure 4c–d, compare blue labeling in each image). Higher magnification images of tumors from animals treated with high dose TMZ showed that fluorescent signal was primarily located in regions of the tumor lacking glioma cells (Figure 5a).

To identify which host cell types might be associated with chemotherapy-induced increases in ProSense labeling, we performed histopathology analyses to assess the degree of host response (macrophages/microglia and neutrophils), tumor proliferation (Ki67), and apoptosis (Tunel) (Figure 5 and data not shown). High dose TMZ treatment increased the number of macrophages/microglia in and around the tumor, but did not affect the number of neutrophils, proliferating cells, or apoptotic cells within the tumor margin (Figure 5b, compare high dose to control, and data not shown). Furthermore, a low dose course of TMZ treatment that was insufficient to alter PAC also did not show an increase in macrophage/microglia recruitment compared to controls (Figure 5b, low dose). Direct co-labeling of ProSense and macrophages/ microglia was not possible due to fluorophore quenching following histology preparation. However, since macrophages are known to up-regulate and secrete ProSense-activating proteases upon recruitment to tumors (Vasiljeva et al., 2006), macrophage/microglia infiltration likely contribute to the increase in PAC seen after high dose TMZ treatment. Thus, these results demonstrate the utility of a FMT-MR combined imaging in the early detection of chemotherapy related changes *in vivo*.

Combined imaging of protease activity to tumor volume is predictive of subsequent tumor growth

Given the ability for combined imaging to detect histopathological changes early in the course of chemotherapy, we wondered whether it was capable of predicting subsequent tumor growth. We treated mice with a low dose regimen (20 mg/kg) and compared them to a high dose regimen (100mg/kg). Whereas low dose treatment resulted in an approximately two-fold increase (one-fold being no increase) in tumor size over the week following chemotherapy (Figure 6a, green bar), high dose treatment was capable of halting tumor growth (1.1-fold increase; Figure 6a, red bar). Tumors treated with either of these doses grew significantly less than untreated tumors (7.2-fold increase, Figure 6a, blue bar).

We next tested whether combined imaging of PAC immediately following TMZ dosing could predict the efficacy of chemotherapy. At the end of the five-day chemotherapy course, PAC was significantly different for low and high dose treatment groups (2730 +/−1020 vs. 10000 +/− 1090 pmol/cm^3, $p=0.0054$). Furthermore, when we plotted the change in tumor volume over the week after chemotherapy versus PAC measured at the end of the chemotherapy course (Figure 6b), we found that there was a significant correlation between these two values ($r=0.79$, $p=0.019$). These results show that measurement of PAC, immediately after chemotherapy, can provide information that is predictive of subsequent tumor growth.

DISCUSSION

In these studies we developed and validated methods to combine tomographic fluorescence imaging and MRI data sets, and applied these methods to monitor the structure and molecular function of living mouse brains. With this approach we observed synchronously the structural and protease activity changes in normal tumor growth and response to chemotherapy *in vivo*. Specifically, FMT-MR imaging revealed the localization of protease activity to solid tumors and allowed for the noninvasive quantification of protease activity concentration in and surrounding tumors. Furthermore, PAC was altered during the course of chemotherapy and allowed for early detection of changes in host response to the tumor that correlated with reductions in tumor growth. These results demonstrate one specific application for combined FMT-MR imaging in the noninvasive monitoring of biological phenomena in living animals.

Combined FMT-MR imaging provides a powerful method by exploiting advantages inherent to each modality. The advantages of fluorescence imaging lie in its quantitative and highly sensitive detection of fluorescent signals (Ntziachristos et al., 2003) and its ability to utilize a wealth of specific molecular probes (Hintersteiner et al., 2005; Izmailova et al., 2007; Jaffer et al., 2006; Kelloff et al., 2005; Nesterov et al., 2005) to detect small changes in cellular and molecular physiology. Conversely, MRI has high spatial resolution and can discretely define the margins of tumors from normal tissue. A combined approach takes the advantages of both modalities and offers the ability to map a broad range of molecular signals onto high resolution anatomical images. To that end, our findings highlight the ability of FMT-MR imaging to reveal physiological information about brain tumors that is not visible by either fluorescence or MR imaging alone. We observed that gadolinium-enhanced MRI, commonly used in drug trials and in clinical imaging, while capable of evaluating tumor morphology and volume, was insufficient to predict tumor response to chemotherapy. On the other hand, a predominately functional approach of FMT imaging, without referencing detailed anatomical structural information, also could not reliably predict the effects of chemotherapy due to the complex host-tumor reactions that arise. Only when we combined the two modalities was critical physiological information (PAC) revealed about the tumors. Supporting the merits of FMT-MR imaging, our method can be used to predict at an early stage whether chemotherapeutic treatment is adequate. FMT-MR imaging therefore could be of broad utility in preclinical trials to better evaluate drug efficacy and optimize drug dosing.

The clinical applications of combined FMT-MR imaging are promising. Theoretical studies suggest that NIRF signals can propagate through large human organs for noninvasive imaging (Ntziachristos et al., 2002b). In addition, fluorescence imaging has been validated for the visualization of normal and diseased human breast tissue (Ntziachristos et al., 2000) suggesting that combined imaging of PAC after chemotherapy might be feasible in a clinical setting. Furthermore, studies of brain irradiation also show significant inflammation (Monje et al., 2003), suggesting that there should be a detectable change in PAC in response to radiotherapy.

Recently, a diffusion weighted MR imaging method (functional diffusion map) has been shown to be highly sensitive and specific in predicting treatment response in brain tumors by examining changes in water movement (Moffat et al., 2005). Our FMT-MR pilot study on tumor treatment response also shows great promise in predicting treatment response, but by examining protease activity. The two methods are complementary, and imaging protocols could be developed to combine both methods to obtain information not available to either method alone. Moreover, given the multitude of fluorescent probes and the general applicability of MRI, FMT-MR imaging could be useful for a variety of new applications. Applications of interest could include the following: 1) similar studies as described here on brain tumor growth and death conducted using different molecular fluorescent probes and/or therapeutic agents, 2) direct visualization and tracking of both tumor cells and therapeutic stem cells labeled with NIRF lipophilic dyes or NIRF proteins (Shcherbo et al., 2007) and 3) study of neurodegeneration utilizing NIRF probes for amyloid-beta (Hintersteiner et al., 2005). Furthermore, FMT-MR imaging need not be limited to the study of the central nervous system. This technique should be useful for applications that are aided by noninvasive, quantitative detection of anatomical and physiological information in living animals-the screening of biomarkers for drug development and disease prognosis provides an immediate example.

Supplementary Material

Refer to Web version on PubMed Central for supplementary material.

Acknowledgments

This work was supported in part by the National Institute of Health 5KO8-HL081170 (J.W.C.) and RO1-EB006432 (R.W.). We thank Y. Iwamato, T. Sponholtz, C. Rangel, C. Kaufman, A. Yu, and J. Chan for experimental assistance, N. Sergeyev for chemical synthesis, and C. Vinegoni, J.C. Tapia, N. Kasthuri and J. Lichtman for useful discussions.

REFERENCES

Bindal AK, Hammoud M, Shi WM, Wu SZ, Sawaya R, Rao JS. Prognostic significance of proteolytic enzymes in human brain tumors. J Neurooncol 1994;22:101–110. [PubMed: 7538161]

Blum G, Mullins SR, Keren K, Fonovic M, Jedeszko C, Rice MJ, Sloane BF, Bogyo M. Dynamic imaging of protease activity with fluorescently quenched activity-based probes. Nat Chem Biol 2005;1:203–209. [PubMed: 16408036]

Brat DJ, Castellano-Sanchez AA, Hunter SB, Pecot M, Cohen C, Hammond EH, Devi SN, Kaur B, Van Meir EG. Pseudopalisades in glioblastoma are hypoxic, express extracellular matrix proteases, and are formed by an actively migrating cell population. Cancer Res 2004;64:920–927. [PubMed: 14871821]

Bremer C, Ntziachristos V, Weissleder R. Optical-based molecular imaging: contrast agents and potential medical applications. Eur Radiol 2003;13:231–243. [PubMed: 12598985]

Graves EE, Yessayan D, Turner G, Weissleder R, Ntziachristos V. Validation of in vivo fluorochrome concentrations measured using fluorescence molecular tomography. J Biomed Opt 2005;10:44019. [PubMed: 16178652]

Hintersteiner M, Enz A, Frey P, Jaton AL, Kinzy W, Kneuer R, Neumann U, Rudin M, Staufenbiel M, Stoeckli M, Wiederhold KH, Gremlich HU. In vivo detection of amyloid-beta deposits by near-infrared imaging using an oxazinederivative probe. Nat Biotechnol 2005;23:577–583. [PubMed: 15834405]

Izmailova ES, Paz N, Alencar H, Chun M, Schopf L, Hepperle M, Lane JH, Harriman G, Xu Y, Ocain T, Weissleder R, Mahmood U, Healy AM, Jaffee B. Use of molecular imaging to quantify response to IKK-2 inhibitor treatment in murine arthritis. Arthritis Rheum 2007;56:117–128. [PubMed: 17195214]

Jaffer FA, Libby P, Weissleder R. Molecular and cellular imaging of atherosclerosis: emerging applications. J Am Coll Cardiol 2006;47:1328–1338. [PubMed: 16580517]

Jiang T, Olson ES, Nguyen QT, Roy M, Jennings PA, Tsien RY. Tumor imaging by means of proteolytic activation of cell-penetrating peptides. Proc Natl Acad Sci U S A 2004;101:17867–17872. [PubMed: 15601762]

Kak, A.; Slaney, M. Principles of Computerized Tomographic Imaging. New York.: IEEE Press; 1988.

Kelloff GJ, Krohn KA, Larson SM, Weissleder R, Mankoff DA, Hoffman JM, Link JM, Guyton KZ, Eckelman WC, Scher HI, O'Shaughnessy I, Cheson BD, Sigman CC, Tatum JL, Mills GQ, Sullivan DC, Woodcock J. The progress and promise of molecular imaging probes in oncologic drug development. Clin Cancer Res 2005;11:7967–7985. [PubMed: 16299226]

Koblinski JE, Ahram M, Sloane BF. Unraveling the role of proteases in cancer. Clin Chim Acta 2000;291:113–135. [PubMed: 10675719]

Lardinois D, Weder W, Hany TF, Kamel EM, Korom S, Seifert B, von Schulthess GK, Steinert HC. Staging of non-small-cell lung cancer with integrated positron-emission tomography and computed tomography. N Engl J Med 2003;348:2500–2507. [PubMed: 12815135]

Moffat BA, Chenevert TL, Lawrence TS, Meyer CR, Johnson TD, Dong Q, Tsien C, Mukherji S, Quint DJ, Gebarski SS, Robertson PL, Junck LR, Rehemtulla A, Ross BD. Functional diffusion map: a noninvasive MRI biomarker for early stratification of clinical brain tumor response. Proc Natl Acad Sci U S A 2005;102:5524–5529. [PubMed: 15805192]

Monje ML, Toda H, Palmer TD. Inflammatory blockade restores adult hippocampal neurogenesis. Science 2003;302:1760–1765. [PubMed: 14615545]

Montet X, Ntziachristos V, Grimm J, Weissleder R. Tomographic fluorescence mapping of tumor targets. Cancer Res 2005;65:6330–6336. [PubMed: 16024635]

Nahrendorf M, Sosnovik DE, Waterman P, Swirski FK, Pande AN, Aikawa E, Figueiredo JL, Pittet MJ, Weissleder R. Dual channel optical tomographic imaging of leukocyte recruitment and protease activity in the healing myocardial infarct. Circ Res 2007;100:1218–1225. [PubMed: 17379832]

Nesterov EE, Skoch J, Hyman BT, Klunk WE, Bacskai BJ, Swager TM. In vivo optical imaging of amyloid aggregates in brain: design of fluorescent markers. Angew Chem Int Ed Engl 2005;44:5452–5456. [PubMed: 16059955]

Ntziachristos V, Bremer C, Graves EE, Ripoll J, Weissleder R. In vivo tomographic imaging of near-infrared fluorescent probes. Mol Imaging 2002a;1:82–88. [PubMed: 12920848]

Ntziachristos V, Bremer C, Weissleder R. Fluorescence imaging with nearinfrared light: new technological advances that enable in vivo molecular imaging. Eur Radiol 2003;13:195–208. [PubMed: 12541130]

Ntziachristos V, Ripoll J, Wang LV, Weissleder R. Looking and listening to light: the evolution of whole-body photonic imaging. Nat Biotechnol 2005;23:313–320. [PubMed: 15765087]

Ntziachristos V, Ripoll J, Weissleder R. Would near-infrared fluorescence signals propagate through large human organs for clinical studies? Opt Lett 2002b;27:333–335. [PubMed: 18007794]

Ntziachristos V, Schellenberger EA, Ripoll J, Yessayan D, Graves E, Bogdanov A Jr. Josephson L, Weissleder R. Visualization of antitumor treatment by means of fluorescence molecular tomography with an annexin V-Cy5.5 conjugate. Proc Natl Acad Sci U S A 2004;101:12294–12299. [PubMed: 15304657]

Ntziachristos V, Tung CH, Bremer C, Weissleder R. Fluorescence molecular tomography resolves protease activity in vivo. Nat Med 2002c;8:757–760. [PubMed: 12091907]

Ntziachristos V, Yodh AG, Schnall M, Chance B. Concurrent MRI and diffuse optical tomography of breast after indocyanine green enhancement. Proc Natl Acad Sci U S A 2000;97:2767–2772. [PubMed: 10706610]

Otsuka H, Morita N, Yamashita K, Nishitani H. FDG-PET/CT for cancer management. J Med Invest 2007;54:195–199. [PubMed: 17878667]

Schiff D. Temozolomide and radiation in low-grade and anaplastic gliomas: temoradiation. Cancer Invest 2007;25:776–784. [PubMed: 17952745]

Shcherbo D, Merzlyak EM, Chepurnykh TV, Fradkov AF, Ermakova GV, Solovieva EA, Lukyanov KA, Bogdanova EA, Zaraisky AG, Lukyanov S, Chudakov DM. Bright far-red fluorescent protein for whole-body imaging. Nat Methods 2007;4:741–746. [PubMed: 17721542]

Sloane BF. Suicidal tumor proteases. Nat Biotechnol 1996;14:826–827. [PubMed: 9631001]

Trehin R, Figueiredo JL, Pittet MJ, Weissleder R, Josephson L, Mahmood U. Fluorescent nanoparticle uptake for brain tumor visualization. Neoplasia 2006;8:302–311. [PubMed: 16756722]

Vasiljeva O, Papazoglou A, Kruger A, Brodoefel H, Korovin M, Deussing I, Augustin N, Nielsen BS, Almholt K, Bogyo M, Peters C, Reinheckel T. Tumor cell-derived and macrophage-derived cathepsin B promotes progression and lung metastasis of mammary cancer. Cancer Res 2006;66:5242–5250. [PubMed: 16707449]

Veit-Haibach P, Kuehle CA, Beyer T, Stergar H, Kuehl H, Schmidt J, Borsch G, Dahmen G, Barkhausen J, Bockisch A, Antoch G. Diagnostic accuracy of colorectal cancer staging with whole-body PET/CT colonography. Jama 2006;296:2590–2600. [PubMed: 17148724]

von Wallbrunn A, Holtke C, Zuhlsdorf M, Heindel W, Schafers M, Bremer C. In vivo imaging of integrin alpha v beta 3 expression using fluorescence-mediated tomography. Eur J Nucl Med Mol Imaging 2007;34:745–754. [PubMed: 17131149]

Weber WA, Grosu AL, Czernin J. Technology Insight: advances in molecular imaging and an appraisal of PET/CT scanning. Nat Clin Pract Oncol 2008;5:160–170. [PubMed: 18253106]

Weissleder R, Ntziachristos V. Shedding light onto live molecular targets. Nat Med 2003;9:123–128. [PubMed: 12514725]

Weissleder R, Tung CH, Mahmood U, Bogdanov A Jr. In vivo imaging of tumors with protease-activated near-infrared fluorescent probes. Nat Biotechnol 1999;17:375–378. [PubMed: 10207887]

Zacharakis G, Kambara H, Shih H, Ripoll J, Grimm J, Saeki Y, Weissleder R, Ntziachristos V. Volumetric tomography of fluorescent proteins through small animals in vivo. Proc Natl Acad Sci U S A 2005;102:18252–18257. [PubMed: 16344470]

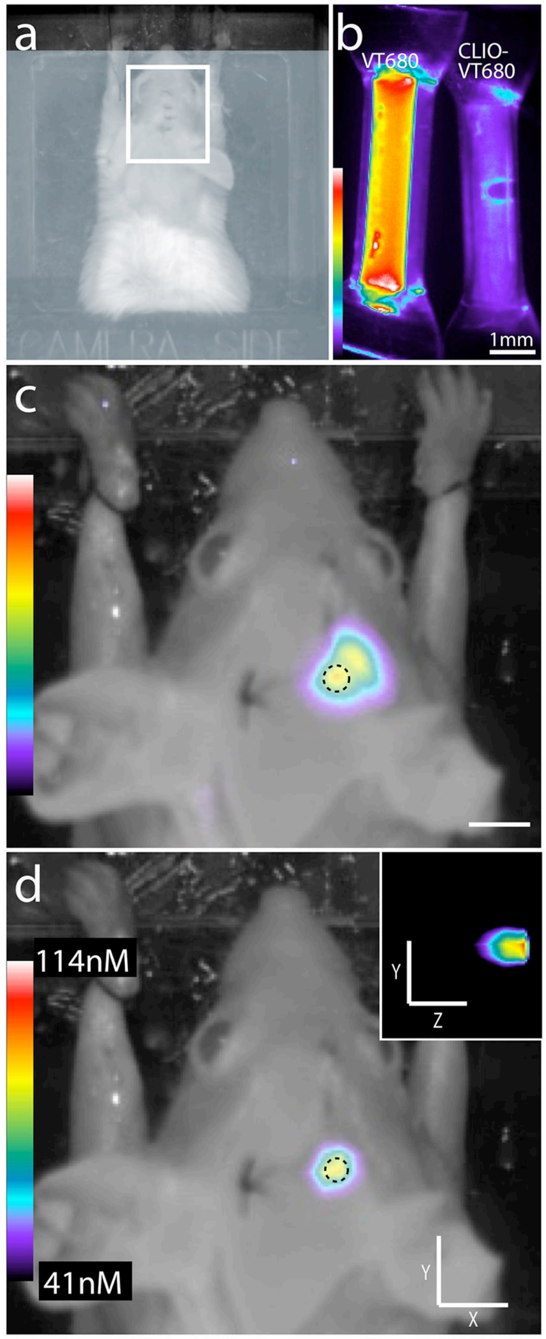

Figure 1. Tomographic fluorescence imaging of the mouse brain *in vivo*

a. Mice were imaged in a fluorescence tomography system. This system requires that the animal be submerged in a refractive index matching fluid. For brain imaging, the animal was suspended so that the nose was above the fluid level (light blue) and the brain area to be imaged was below it (white square). ***b***. Plastic phantoms were filled with a NIRF fluorophore (*VT680*) or magnetofluorescent particles (*CLIO-VT680*). Phantoms were implanted into the brains of living mice for fluorescence tomographic imaging. ***c***. Transmitted fluorescence imaging (TFI) of an animal with a single fluorescent phantom. Actual phantom size is represented by the *dashed black circle*. Note that TFI provides neither fluorophore concentrations nor 3d data. ***d***. When we imaged animals with a single implanted phantom (outlined by the dashed black circle), we were able to detect a single fluorescent focus (see also *inset* for sagittal projection). Fluorophore concentrations could be extracted from this data set. Scale bar equals 3mm.

NIH-PA Author Manuscript
NIH-PA Author Manuscript

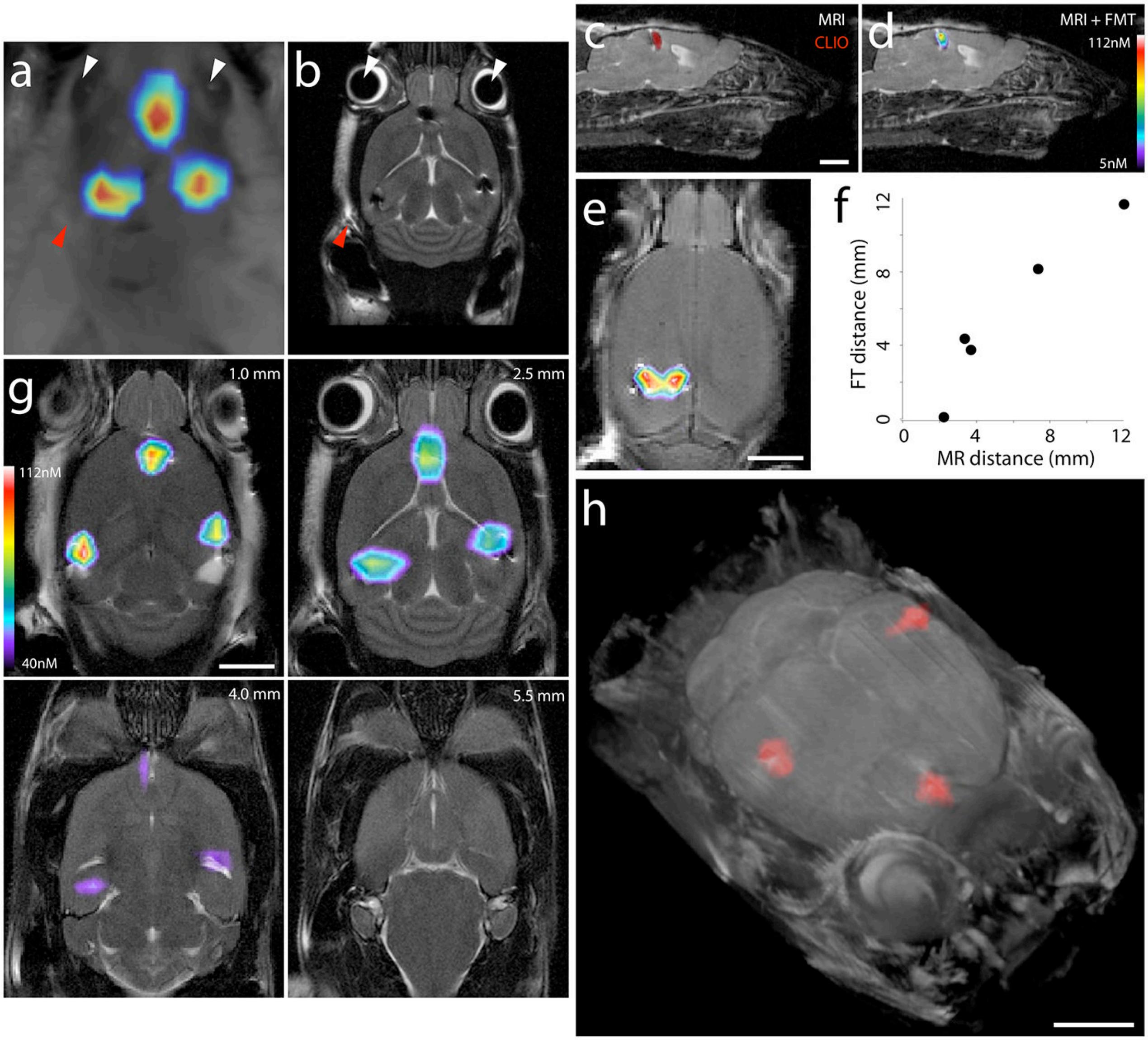

Figure 2. Combined fluorescence and magnetic resonance imaging

By implanting phantoms filled with magnetofluorescent particles, we were able to image the same animals with fluorescence tomography and MRI. ***a***. After imaging, fluorescence and MR datasets could be manually aligned using anatomical landmarks common to both images. Shown here is an example of a fluorescence tomography image that has been automatically fused to a reflectance image by the FMT software. Structures like eyes (*white arrows*) and ear (*red arrow*) can be identified in this image and aligned with the same structures in corresponding MR images (see corresponding arrows in ***b***). ***c***. A single phantom can be detected as a hypointense region (*colorized red*) on MRI. ***d***. Fluorescence concentrations from fluorescence tomography imaging could then be mapped onto the MR images. See Figure S1 for a 3D projection of the animal depicted in *c* and *d*. ***e***. FMT-MR imaging was also possible in animals with more than one magnetofluorescent phantom. Shown here is an animal with two phantoms implanted 4mm apart. ***f***. Fluorescence and MR measurements of phantom separation correlated up to 4mm. Each data point represents an individual animal with multiple phantoms implanted at varying distances. ***g***. To determine the feasibility of 3D image fusion, we implanted three magnetofluorescent phantoms into a living mouse, imaged it with fluorescence tomography and MR and then fused the imaged by triangulating in 3D space. Shown here are fused images arranged from superficial cortex to deeper brain regions. Measurements in the upper right corner equal the distance from the surface of the skull. ***h***. Three dimensional volume rendering of the fused dataset from (*g*). Scale bars equal 3mm in all images.

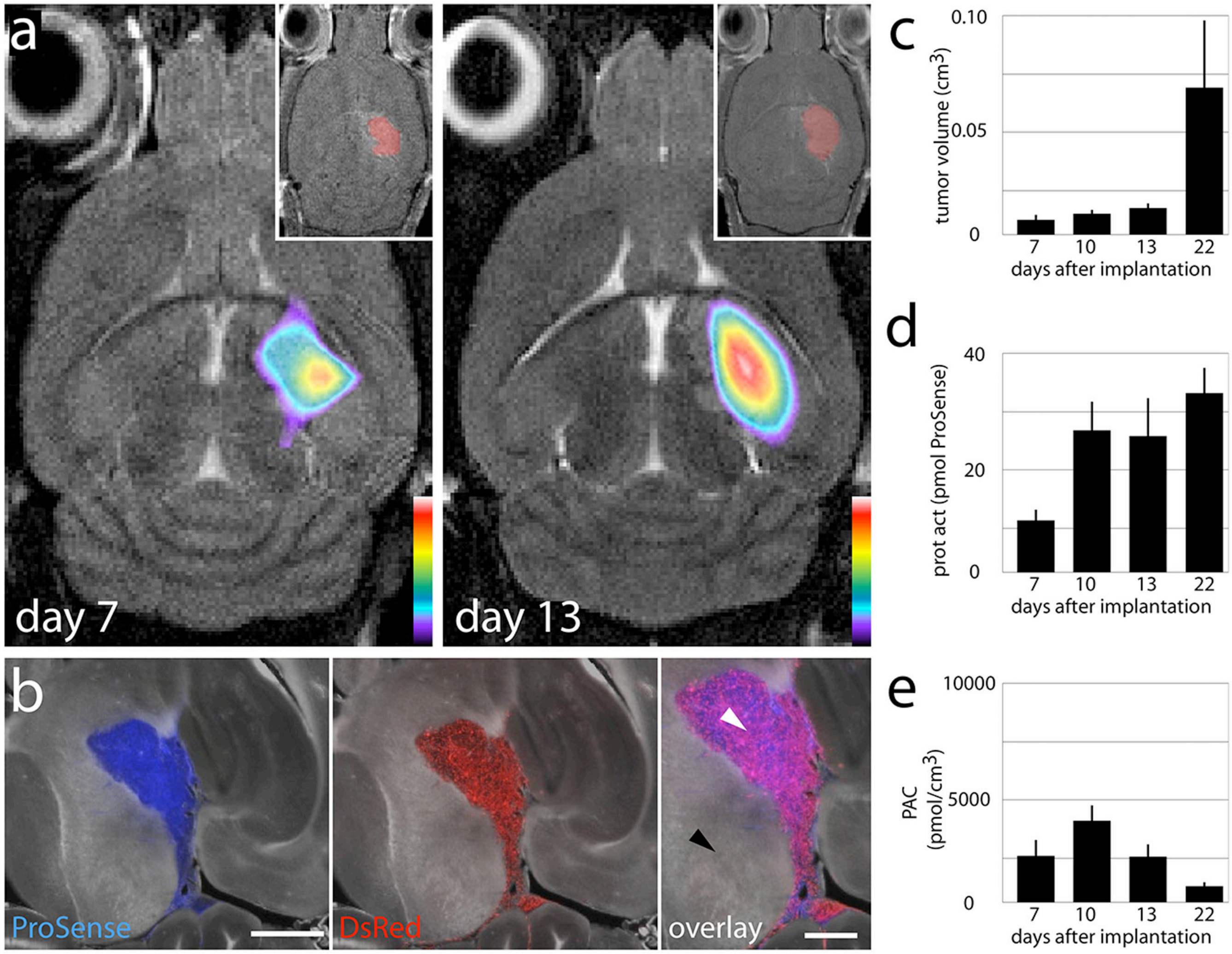

Figure 3. Combined fluorescence and MR imaging of brain tumors

a. ProSense, an activatable fluorescent probe for protease activity, was injected intravenously into glioma-bearing nude mice. FMT of these mice revealed focal presence of protease activity. On Gd-enhanced MR images (inset---Gd enhancing region pseudocolored red), we could determine glioma size and location. Fluorescent tomographic images of protease activity could then be mapped onto the MR images to reveal protease activity associated with the glioma. Shown here are representative combined images at 7 and 13 days after glioma implantation. ***b***. Fluorescence microscopy of a typical mouse at day 13 after glioma implantation. ProSense fluorescence (blue, panel 1) localized to the DsRedII-expressing tumor cells (red, panel 2; white arrow, panel 3), but was not found in brain regions not bearing glioma cells (black arrow, panel 3). Scale bar equals 0.5mm. ***c-e***. Quntification of brain tumor imaging. ***c***. Tumor volume, measured with MRI, was observed to increase over the course of 3 weeks.***d***. Protease activity, measured by FMT imaging of ProSense fluorescence signal, increased over the same time period. ***e***. Using combined imaging, we could calculate protease activity concentration (PAC). In the untreated tumors, PAC showed an early increase (*see day 10*) and then decreased for the remainder of the 3-week course of imaging.

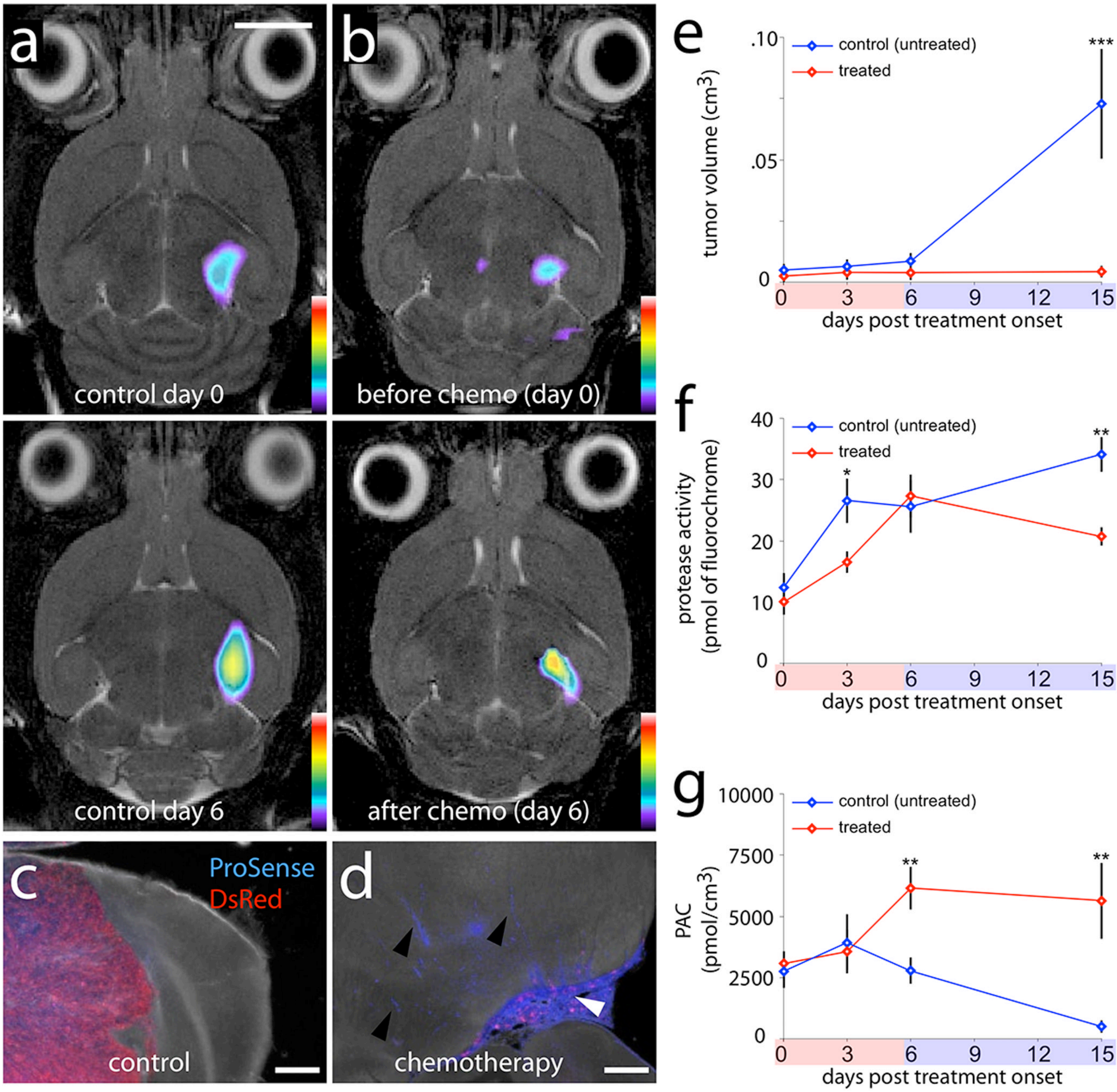

Figure 4. Chemotherapy increases the ratio of protease activity to tumor volume

Control and chemotherapy treated animals received the same number of glioma cells one week prior to imaging. At that point, they were assigned to either the control or chemotherapy group. Chemotherapy (temozolomide) was given to the treatment group for 5 days and then all animals were imaged over time. ***a***. Combined FMT-MR imaging of a mouse bearing an implanted glioma. ***b***. Combined FMT-MR imaging of a chemotherapy treated mouse bearing a similarly sized glioma. Note that the protease activity appears to be denser than in the control animal. ***c***. In control animals, ProSense fluorescence (*blue*) localized to the tumor (*red*) and did not extend beyond the tumor margin. ***d***. In chemotherapy treated animals, ProSense fluorescence was present both inside the tumor (*white arrow*) as well as outside of the tumor (*black arrows*). Scale bars equal 0.5mm. ***e-f***. Quantification of the effects of chemotherapy on protease activity and tumor size. The abscissas represent the duration of chemotherapy treatment (*shaded in red*) and the subsequent follow up time (*shaded in blue*). ***e***. Tumor volume, measured with MRI, increased exponentially over the course of 2 weeks. The difference between control and treatment groups was significant only after day 6 after chemotherapy. ***d***. Protease activity, showed a significant decrease by three days of treatment, but there was no significant difference between control and treatment groups by the end of the chemotherapy regimen. By day 15, control tumors showed significantly more protease activity than chemotherapy treated tumors. ***e***. PAC was significantly altered by the end of a 5 day course of chemotherapy. This difference became even more pronounced at the end of the experiment (day 15 after chemotherapy).

NIH-PA Author Manuscript

NIH-PA Author Manuscript

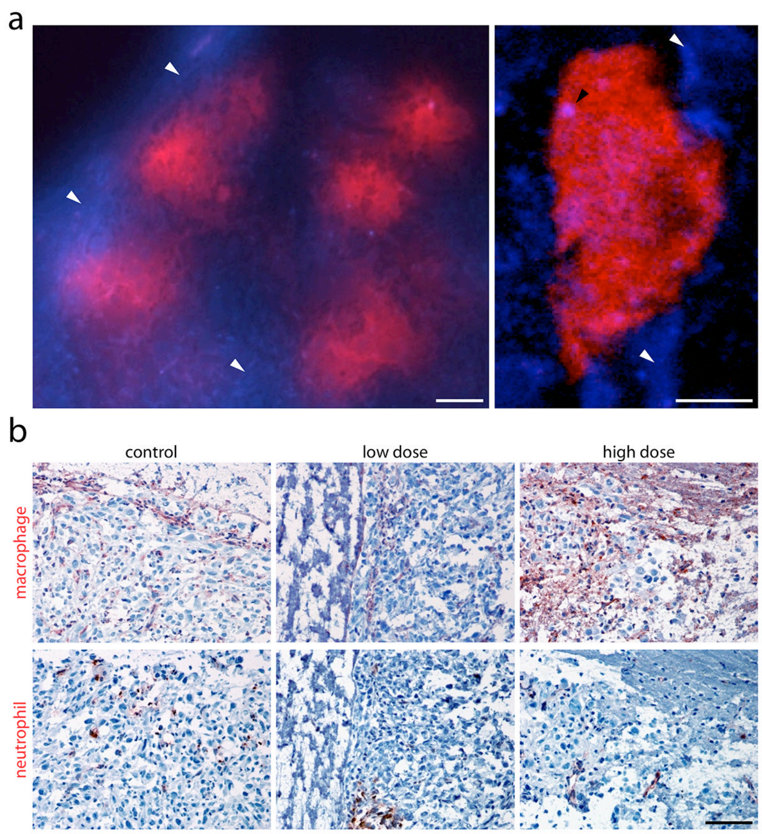

Figure 5. Macrophage infiltration of gliomas following high dose chemotherapy treatment

Images depict sections through the largest identifiable region of tumor growth. ***a***. *Left*. High magnification fluorescent microscopy images of DsRedII expressing tumors after systemic high dose chemotherapy. ProSense labeling (*blue*) was most intense in regions lacking glioma cells (*red*) (*white arrows*). *Right*. High magnification view of a single labeled tumor cell. ProSense labeling was present in small puncta contained within the tumor cell border (*black arrow*) but most of the ProSense signal was located outside of tumor cells (*white arrows*). Scale bar equals 100µm in left panel and 5 µm in right panel. ***b***. Top row. Antibody staining for macrophages (*red*) showed increased labeling after high dose chemotherapy (compare left and right images) but did not show markedly increased labeling following low dose chemotherapy (compare left and middle images). Bottom row. Antibody staining for neutrophils (*red*) did not reveal many neutrophils in or around the tumors, or any difference between control, low dose, or high dose treatments. Scale bar equals 100µm.

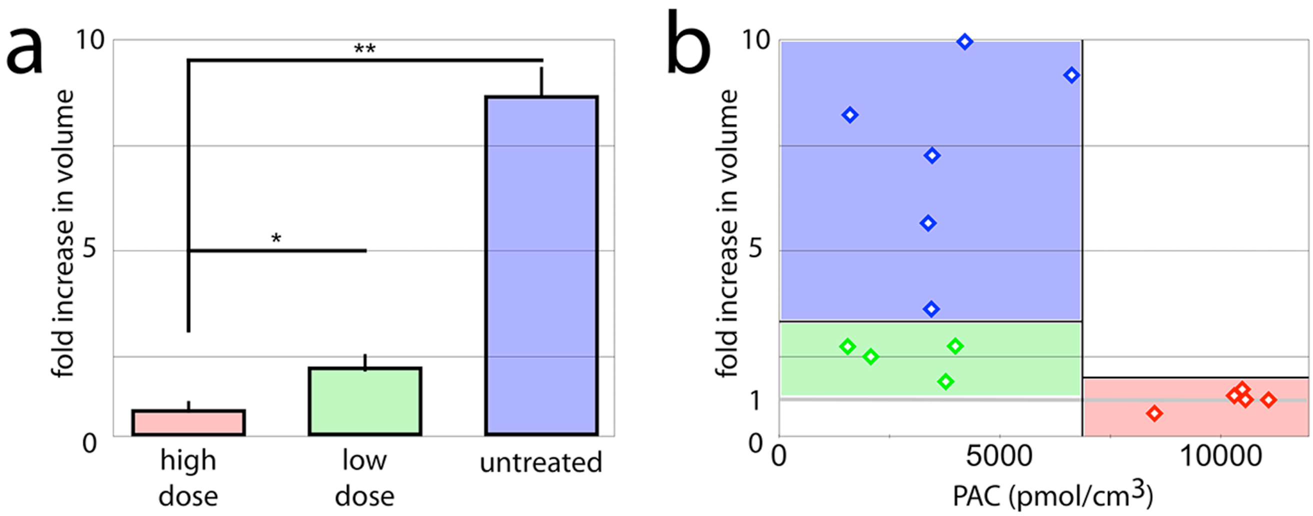

Figure 6. Ratio of protease activity to tumor volume is predictive of subsequent tumor growth

a. The amount of tumor growth (as assayed by MRI) in the week following cessation of chemotherapy varied with the chemotherapeutic dose. High dose (*red*) and low dose (*green*) represent chemotherapy doses in mouse that mimic human high and low dose clinical treatment courses. *Fold increase in tumor volume* refers to the change in tumor volume from the end of chemotherapy until one week later (in *a* and *b*). ***b***. PAC measured at the end of the 5 day chemotherapy course, was predictive of the amount of tumor growth over the week following chemotherapy. Each diamond represents data from a single animal. Animals treated with a high dose of chemotherapy (*red diamonds*) showed the highest amount of protease activity per tumor volume at the end of the chemotherapy treatment course. One week later, they also showed no or minimal growth (1 fold increase represents no new growth). In contrast, animals treated with low dose chemotherapy (*green diamonds*) showed similar protease activity to tumor volume as untreated controls (*blue diamonds*) and grew significantly more than brain tumors in the high dose group.